




Electrochemical malathion sensors based on phytic acid-doped polyaniline and overoxidized polyaniline nanorods

Chunming He¹, Ru Yan^{1*} , Qingwang Xue¹, Shuxian Li¹, and Huaisheng Wang^{1,*}

¹Department of Chemistry, Liaocheng University, No.1 Hunan Road, Liaocheng 252059, Shandong, China

Received: 8 October 2022

Accepted: 1 December 2022

Published online:

1 January 2023

© The Author(s), under exclusive licence to Springer Science+Business Media, LLC, part of Springer Nature 2022

ABSTRACT

In this work, polyaniline (PANI) and overoxidized polyaniline (oPANI) nanorods doped by phytic acid (PA) with uniform size of 60–100 nm were prepared and modified on glassy carbon electrode (GCE) as non-enzymatic malathion sensors. Doping of PA has deep influence on structural and morphological properties, conductivity and detection performance of electrode materials. The obtained PANI nanorods doped with PA (PA-PANI) possess high affinity toward malathion, and thus the redox reaction of PANI molecules could be hindered and redox currents were inhibited. The electrode reaction process on PA-PANI/GCE is a typical adsorption-controlled process. By contrast, the oPANI nanorods doped with PA (PA-oPANI) presents good catalytic performance to malathion and the electron transfer process was enhanced and redox currents increased. Correspondingly, the electrochemical reduction process on PA-oPANI/GCE is a typical diffusion-controlled process. Both enzyme-free electrochemical sensors exhibit good stability, anti-interference ability, recovery in real samples and excellent detection performance, with a wide linear range of 0.01–200 ppb and low detection limit (1.58 ppt for PA-PANI and 2.23 ppt for PA-oPANI, respectively), indicating that PA-PANI and PA-oPANI could be used as an excellent malathion sensor. Moreover, the PA-oPANI sensor has some degree of reproducibility through further anodic polarity processing, and the detailed application needs to be further explored.

Handling Editor: Maude Jimenez.

Address correspondence to E-mail: yanru@lcu.edu.cn; hswang@lcu.edu.cn

Introduction

Malathion is a common organophosphorus pesticide (OPs), which is often used to control crop diseases and insect pests in modern agriculture. However, malathion has high toxicity, and is easily enriched in soil and water, which threatens the security of agricultural products and resources. It's probably worth noting that drinking water or produce containing excessive malathion residues can be harmful to the human nervous system and thus harm human health [1–3]. The commonly used detection methods of organophosphorus pesticides include gas chromatography (GC), high performance liquid chromatography (HPLC), mass spectrometry (MS), etc. These methods have been developed for a long time, and have high sensitivity. However, complicated operation procedures may affect the reliability of test results, and complex equipment may lack flexibility, which limit their application scope [4–8]. Therefore, it is very urgent and has important practical significance to develop a simple and convenient method for rapid detection of malathion. Compared with traditional methods, electrochemical analysis has attracted the attention of researchers because of its low cost, simple operation and high sensitivity. In recent years, electrochemical detection methods have been widely used in environmental monitoring, pesticide residue detection and other fields [9–12].

Currently, the reported electrochemical sensors for organophosphorus pesticides can be mainly divided into two types: enzyme type and non-enzyme type. Although the development of enzyme-type electrochemical sensors for agricultural residues is earlier than that of non-enzyme type, its popularization and application are still limited by the disadvantages of poor stability of enzymes, demanding reaction conditions and high price [13–15]. For this reason, the development of electrochemical sensors for non-enzymatic OPs has attracted more and more attention. A large number of studies have been reported on the application of various metals/metal oxides, metal oxide–carbon nanotube composites and composite nanomaterials in the construction of electrochemical sensors for the detection of pesticide. For example, Gao et al. studied the simultaneous detection of carbendazim and methyl parathion by electrochemical sensors driven by electroactive gold nanopores [16]. Zhang et al. prepared a biosensor based on

conjugated polymer and Ag-RGO-NH₂ nanocomposite material, which can detect malathion and trichlorfon. The detection limit of malathion is about 0.032 µg/L [17]. However, most of these studies focus on noble metals such as Ag and Au or metal oxides with complicated preparation methods. Therefore, other materials for the electrode modification with comparable properties, low-cost and easy availability need to be developed.

Conducting polymers, such as polypyrrole, polyaniline and polythiophene can form different nanostructures like nanofibers, nanotubes and nanospheres through its molecular self-assembly and have great potential for the fabrication of sensors due to their moldable electrical conductivity, chemical stability, the high surface to volume ratio and ease of preparation. Generally speaking, conducting polymers can be used as the mediator for enzyme electrodes. Li et al. fixed acetylcholinesterase on a polyaniline/graphene composite film to modified glassy carbon electrode, which could detect carbaryl at a concentration of 38–194 ng/mL. The detection limit of the electrochemical sensor is 20 ng/mL [18]. Yang et al. mixed gold, polypyrrole and reduced GO sheet, and then fixed acetylcholinesterase on the composite material to detect the paraoxon-ethyl in the range of 1–5 µM. The detection limit of this electrochemical sensor is 0.5 nM [19]. However, there are few reports on the application of conducting polymers as enzyme-free electrochemical sensor in the detection of malathion. Herein, we proposed an enzyme-free electrochemical sensor for malathion detection based on conducting polymers.

Polyaniline (PANI) is one of the important polymer materials with special electrical and optical properties among all various conducting polymers. Due to different reaction conditions, polyaniline exists in different forms, mainly in four states: full reduction state, intermediate state, peroxide state and complete oxidation state. The fully reduced full benzene structure and the fully oxidized full quinone structure are basically insulators with poor electrical conductivity [20, 21]. Therefore, we select the intermediate state and peroxide state of PANI as candidate materials to modify the electrode. The conductivity of polyaniline can be further controlled by proton doping or conventional redox doping based on its property of modifiable electrical conductivity. Phytic acid extracted from cereal grains and seeds is a cyclic acid molecule saturated with

dihydrogen hexaphosphate. As an environmentally friendly, inexpensive, natural and nontoxic organic acid, phytic acid is considered to be an excellent dopant to further improve conductivity and electrochemical performance of PANI [22, 23].

To our best knowledge, there are no cyclic voltammetry methods that have been published for the determination of malathion based on the effect of malathion on the redox property of PANI. In this work, electrochemical sensors based on PA-doped polyaniline nanorods (intermediate polyaniline and peroxidation polyaniline) were prepared for the detection of malathion and different detection mechanisms in the two states were reported. The intermediate polyaniline doped by PA has great capabilities in adsorption of malathion and the electrochemical response currents were inhibited, but the peroxidation polyaniline doped by PA has great electrocatalytic performance in the detection of malathion and the electrochemical response currents were enhanced with the increasing of malathion concentration. In addition, both enzyme-free electrochemical sensors based on PA-doped PANI present a wide linear range (0.01–200 ppb) and excellent reproducibility and favorable selectivity.

Experimental section

Materials and reagents

Malathion, methyl parathion, carbendazim is purchased from J&K Scientific Ltd. (China) and is configured with anhydrous ethanol in a standard solution of a certain concentration. Aniline, phytic acid (50 wt% in water), ammonium persulfate, ascorbic acid and cysteine were purchased from Aladdin Ltd. (Shanghai, China), while anhydrous ethanol, disodium hydrogen phosphate (Na_2HPO_4), citric acid ($\text{C}_6\text{H}_8\text{O}_7$), calcium chloride (CaCl_2), magnesium chloride (MgCl_2), sodium chloride (NaCl), potassium nitrate (KNO_3), potassium sulfate (K_2SO_4), potassium carbonate (K_2CO_3) and potassium chloride (KCl) were purchased from Sinopharm Chemical Reagent Co., Ltd. (Shanghai, China). All reagents in the experiment were analytically pure, and all aqueous solutions were prepared with distilled water.

Synthesis of PA-PANI composites

0.46 mL phytic acid (50 wt % in H_2O) and 0.45 mL aniline monomer were added to 2 mL ultra-pure water and stirred evenly to obtain solution A. 0.285 g ammonium persulfate (APS) was added into 1 mL ultrapure water and mixed evenly to obtain solution B. Solution B was added to solution A and stirred at room temperature for 1 min to obtain a dark green polymer. The obtained polymer was reacted at 4 °C for 24 h at low temperature to ensure that the polymerization reaction was complete, then removed and washed with ultrapure water 2–3 times until the supernatant obtained by centrifugation was transparent. Finally, drying them for 24 h in a vacuum environment at 60 °C, and PA-PANI nanocomposites were obtained.

Preparation of PA-PANI/GCE and PA-oPANI/GCE

1 mg of PA-PANI composite was added into 1 mL ultrapure water and the mixed solution were ultrasonicated for 30 min to obtain homogenous suspension. Before modification, the glassy carbon electrode (GCE) was ground to a smooth surface with Al_2O_3 powder. Then, the glassy carbon electrode was ultrasonic washed with 1:1 HNO_3 , anhydrous ethanol and secondary water for 5 s, and dried at room temperature. Then 10 μL of PA-PANI dispersed solution was casted onto the surface of electrode and dried with an infrared lamp to obtain phytic acid-polyaniline-modified glassy carbon electrode (PA-PANI/GCE).

PA-PANI/GCE was peroxidized by anodic polarization method. A three-electrode system was selected, PA-PANI/GCE prepared in the previous step was used as the working electrode, saturated calomel electrode as the reference electrode, platinum electrode as the counter electrode, and the peroxide experiment was carried out in 0.1 M KCl solution. Cyclic voltammetry (CV) was used to sweep 60 cycles between 0 and 1 V potentials at a speed of 50 mV/s, as shown in Suppl. Fig. S1. After scanning, the working electrode was taken out and washed with ultrapure water to obtain phytic acid-doped polyaniline electrode in peroxide form (PA-oPANI/GCE).

Characterization and electrochemical measurements

The surface morphology, crystal structure and chemical composition of the PA-PANI, PA-oPANI composite were characterized by SEM (Thermo Scientific FIB-SEM GX4), XRD (SmartLab 9 KW X-ray Diffractometer, Japan), XPS (Escalab Xit electron Spectrometer, USA) and IR (Nicolet iS50). The band gaps of PA-PANI and PA-oPANI composite were measured and calculated using a UV–visible spectroscopy (Shimadzu UV-3600 Plus, Japan).

CV and electrochemical impedance spectrum (EIS) were performed at room temperature using CHI 660E electrochemical station. A three-electrode system consisting of PA-PANI/GCE and PA-oPANI/GCE working electrodes, Ag/AgCl reference electrode and platinum counter electrode was used. CV was recorded over the scanning potential range of -0.8 to $+0.8$ V under the scanning rate at 100 mV/s. 30 mL of disodium hydrogen phosphate and citric acid buffer with pH 6.8 was used as the supporting electrolyte. EIS was carried out in the frequency range of 100000 – 0.1 Hz at the potential of 0 V and the amplitude of 5 mV with the electrolyte solution of 0.1 M KCl containing 5.0 mM $[\text{Fe}(\text{CN})_6]^{3-/4-}$. The material preparation and measurement process are presented in Scheme 1.

Actual sample detection

In order to study the applicability of PA-PANI/GCE and PA-oPANI/GCE in the real sample detection toward MP, the electrochemical detection of MP in lake water samples was carried out. The lake water

was obtained from East Lake of the Liaocheng University, Shandong, China and let it stand for one night to remove all the solid impurities. The processed water samples were spiked with different amounts of malathion and detected by CV tests. The concentration of MP in lake water samples were confirmed through the calibration curve obtained from CV experiments.

Results and discussion

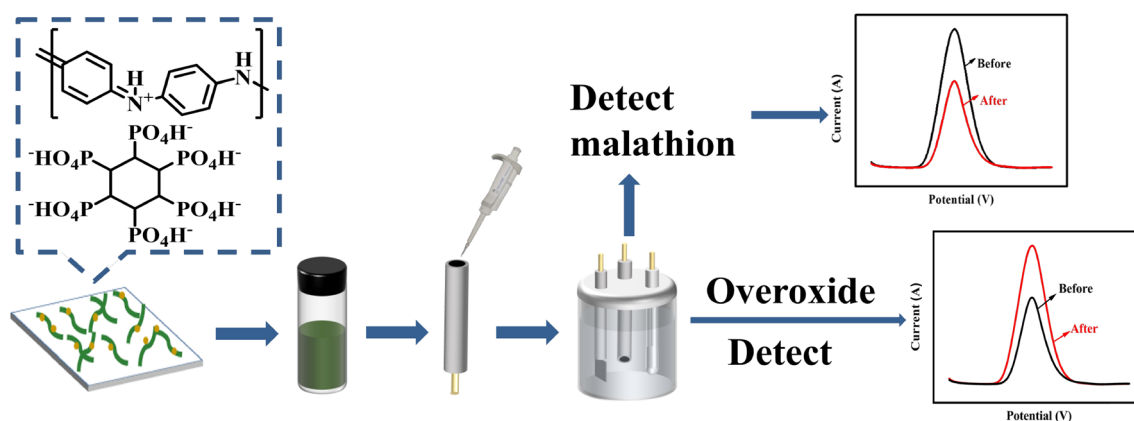
Characterization of PA-PANI and PA-oPANI composite

SEM analysis

The morphological character of the as-synthesized samples was analyzed by SEM. The images of PANI in Fig. 1A, B presents a lamellar structure. After doping by phytic acid, morphology of PANI changed from sheet to rod with the diameter of 60 – 100 nm. PA-PANI nanorods were densely interwoven and the structure became denser in Fig. 1C, D. The SEM images of PA-oPANI in Fig. 1E, F displayed a similar morphology to that of PA-PANI, suggesting that the peroxidation process has little effect on its morphology features.

XRD and IR analysis

XRD patterns of free PANI and PA-doped PANI samples are presented in Fig. 1G. The XRD patterns of PANI show two sharp diffraction peaks with centers of $2\theta = 20.1^\circ$ and 25.4° , indicating the low crystallinity of the material, corresponding to the



Scheme 1 Schematic illustration for the fabrication of PA-PANI/GCE, PA-oPANI/GCE and the electrochemical detection of malathion.

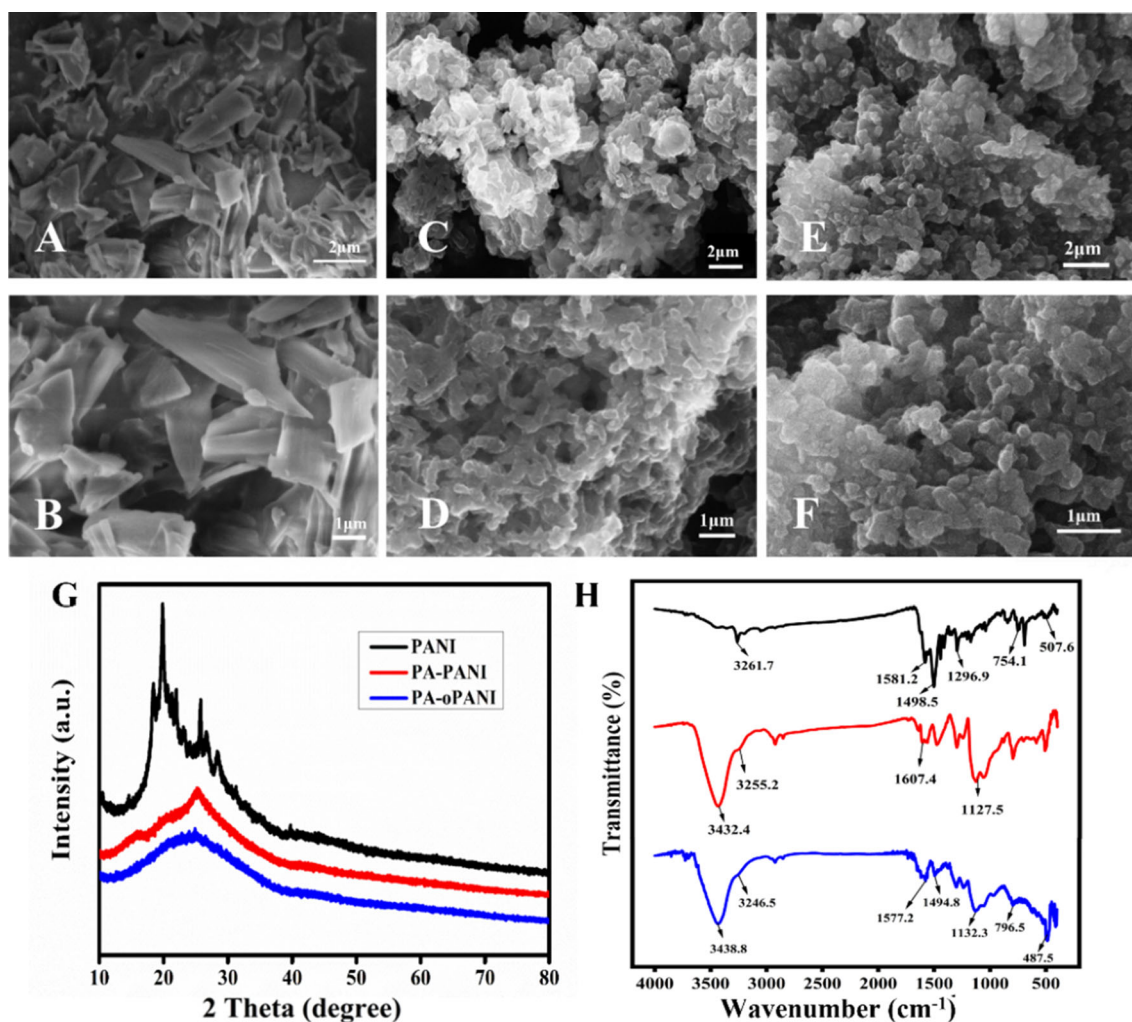


Figure 1 SEM images of PANI (A, B); PA-PANI (C, D); PA-oPANI (E, F), and XRD pattern (G), and FTIR spectra (H) of PANI, PA-PANI, PA-oPANI.

vertical and parallel periodicity of the polymerization backbone in PANI [24], respectively. Compared to PANI, there is only a wide diffraction peak at $2\theta = 25.1^\circ$ for the PA-PANI and PA-oPANI, indicating that the doping of phytic acid has an effect on the crystallinity of PANI. The FTIR spectra of PANI and PA-doped PANI samples are shown in Fig. 1H. The main characteristic peaks of PANI sample were located at 3261.7 cm^{-1} (N–H stretching vibration), 1581.2 and 1494.8 cm^{-1} (C–C stretching vibration of quinoid and benzenoid), 1296.9 (C–N stretching vibration of benzenoid), 754.1 and 507.6 cm^{-1} (bending vibration of C–H on the aromatic ring). After functionalization with phytic acid, the FTIR spectrum still presented main characteristic peaks of PANI, while some new characteristic peaks around 3400 , 1060 , 1130 cm^{-1} attributed to the stretching

vibrations of –OH, P–O and P=O bonds appeared [25, 26]. The result indicated that PANI were successfully doped with PA, and peroxidation process has little effect to its chemical components.

XPS and band gap energy analysis

XPS was used to study the chemical states of elements in PANI and PA-doped PANI samples. The XPS survey spectra and high-resolution deconvoluted spectra of the C1s, N1s and P2p peaks are shown in Fig. 2 and Suppl. Fig. S2. The XPS survey spectra of PANI sample present three characteristic peaks from C, N and O element. Compared to the obtained PANI spectra, the new characteristic peak from P element confirmed the presence of PA in the doped PANI samples. In order to have a better

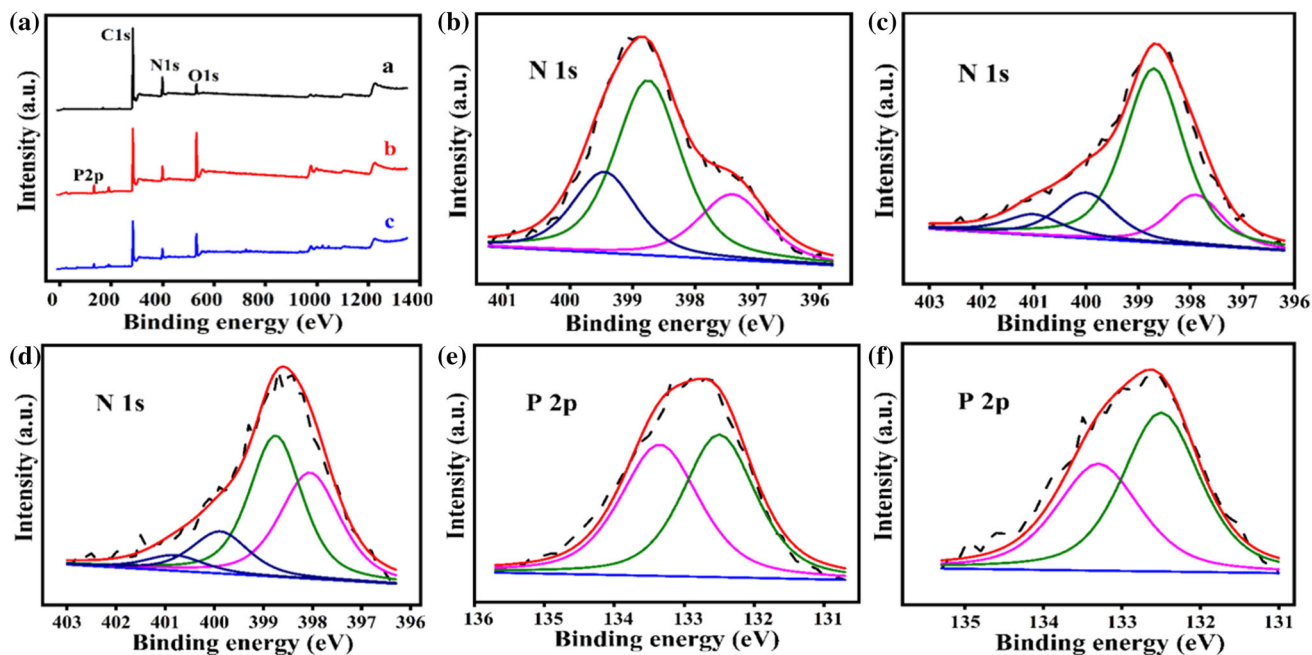


Figure 2 XPS survey spectra (A) of PANI (a), PA-PANI (b) and PA-oPANI (c), high-resolution N1s spectra of PANI (B), high-resolution N1s, P2p spectra of PA-PANI (C, E), high-resolution N1s, P2p spectra of PA-oPANI (D, F).

understanding about the doping behavior of PANI, further analysis for high-resolution spectra of C, N, O and P element were carried out. For the PANI sample, its C1s spectra can be fitted into three peaks located at 283.5, 284.4 and 285.6 eV, which are associated with C=C, C-C and C-N bonds (see Suppl. Fig. S2). The high-resolution N1s spectra displayed three obvious components centered at 397.9, 398.7 and 400.1 eV ascribed respectively to imines N (-N=), benzenoid diamine N (-NH-) and amine (N-H). For PA-PANI sample, its high-resolution deconvoluted spectra of the C1s still presented three obvious components assigned to C=C, C-C and C-N bonds. The high-resolution P2p spectra consists of two significant peaks at 133.3 eV and 132.5 eV, which are related to oxidized phosphorus atoms [27–31]. However, the high-resolution N1s spectra revealed another new component located at 401 eV assigned to positively charged aniline (-NH^{*+}-) [32, 33]. The XPS results confirmed that PA molecules are bound by PANI through electrostatic interaction. For PA-oPANI sample, the high-resolution C1s, N1s and P2p spectra exhibited same components with that of PA-PANI sample. It is worth noting that composition of imines N (-N=) in N1s spectra increased obviously after anodic polarization process, which can be

judged by increased area of peak at 397.9 eV in Fig. 2D. It gave direct evidence that peroxidation process was successfully carried out and PA-oPANI sample was obtained.

The band gap of conducting polymers, defined as the least photon energy needed for exciting an electron from the highest occupied molecular orbital (HOMO) to the lowest unoccupied molecular orbital (LUMO), can be used as an important indicator to evaluate the conductivity of electrons of conducting polymers. A low band gap energy means that electron transitions are easier and the material has a stronger conductivity [34, 35].

Herein, the band gap energy of PA-PANI and PA-oPANI composite was measured and calculated by means of the tauc plot in Suppl. Fig. S3 and tauc equation reported in previous work [36]. According to Suppl. Fig. S3, the band gap energy of PA-PANI and PA-oPANI has been calculated as 2.6 and 3.25 eV respectively. PA-PANI composite possessed lower band gap energy and higher conductivity. Peroxidation process resulted in increased band gap and decreased conductivity for PA-oPANI composite. It also offered an indirect proof of successfully peroxidation for PA-PANI composite.

Electrochemical properties

The electron transfer characteristics of the bare GCE electrode and modified GCE electrodes by PANI-based materials was studied using CV and EIS in 0.1 M KCl solution containing 5 mM $[\text{Fe}(\text{CN})_6]^{3-}$, with those results shown in Fig. 3A and Suppl. Fig. S4. Compared with GCE, the redox currents of $[\text{Fe}(\text{CN})_6]^{3-}$ at PA-PANI/GCE and PA-oPANI/GCE increase significantly but decreased lightly at the PANI/GCE. It revealed that PA-PANI and PA-oPANI can accelerate the electron transfer between $[\text{Fe}(\text{CN})_6]^{3-}$ and electrode surface, thus increased the electrode conductivity, while PANI hindered the ability of partial electron transfer due to its low conductivity. The PA-PANI material had the greatest positive impact on the increase in conductivity. When PA-PANI was further oxidized through electrochemical method, the redox currents of $[\text{Fe}(\text{CN})_6]^{3-}$ decreased significantly, which indicated that anodic polarization could turn the PA-PANI into PA-oPANI with a large loss of electroactivity. The result is consistent with that of band gap energy.

EIS was further carried out to evaluate the impedance change of modified GCE. As shown in Fig. 3B and Suppl. Fig. S4, the Nyquist plots of bare GCE and modified GCE all presented incomplete semicircle related to dynamics behavior at high frequency and an oblique line associated with diffusion control process at low frequency. Generally, the diameter of the semicircle is approximately equal to the charge transfer resistance (R_{ct}). The larger semicircle diameter, the higher value of R_{ct} and the worse conductivity will be. Therefore, the electron transfer ability of bare GCE and modified GCE can be determined on the basis of the capacitive loop diameters. It can be

ranked in the following order: PA-PANI/GCE > PA-oPANI/GCE > GCE > PANI/GCE, demonstrating that the modification of PA-PANI or PA-oPANI effectively improved the conductivity of GCE, while the PANI has the negative effect on electron transfer ability.

CV measurements were performed to study electrochemical behavior of GCE electrode and PANI-based materials modified electrodes in 0.1 M Na_2HPO_4 -citrate buffer solution (pH = 6.8) in the absence and presence of 40 ppb malathion. As displayed in Fig. 4, no obvious peaks were observed at the bare GCE and PANI/GCE, while strong cathodic peak ascribed to the valence changes of PANI around -0.2 V can be found for PA-PANI/GCE and PA-oPANI/GCE. What's more, the PA-PANI/GCE and PA-oPANI/GCE presented higher current response as well as larger current change after addition of malathion compared to that of bare GCE and PANI/GCE. This result indicated that the doping of PA molecules in PANI is conducive to enhancement of electrical conductivity and electrochemical sensing ability due to the synergistic effect between PA and PANI. However, it should be noted that mechanism of the electrode reaction was different for PA-PANI and PA-oPANI modified electrodes. The current decreased for PA-PANI/GCE but increased for PA-oPANI/GCE after addition of malathion, and further investigation is needed.

The amount of PA doping in both PANI and oPANI is the important parameter that affects the current response and the sensitivity of the electrochemical detection. As it is visualized in Suppl. Fig. S5, the change rate of response current presented an obvious dependence on the doping amount of PA. The current response increased with the increasing

Figure 3 CVs at a sweep rate of 100 mV s^{-1} (A) and Nyquist diagrams of PA-PANI/GCE and PA-oPANI/GCE (B) in 0.1 M KCl containing 5.0 mM $[\text{Fe}(\text{CN})_6]^{3-/4-}$: PA-PANI/GCE (a) and PA-oPANI/GCE (b). Inset: CV curve (a) and Nyquist diagram (b) of bare GCE.

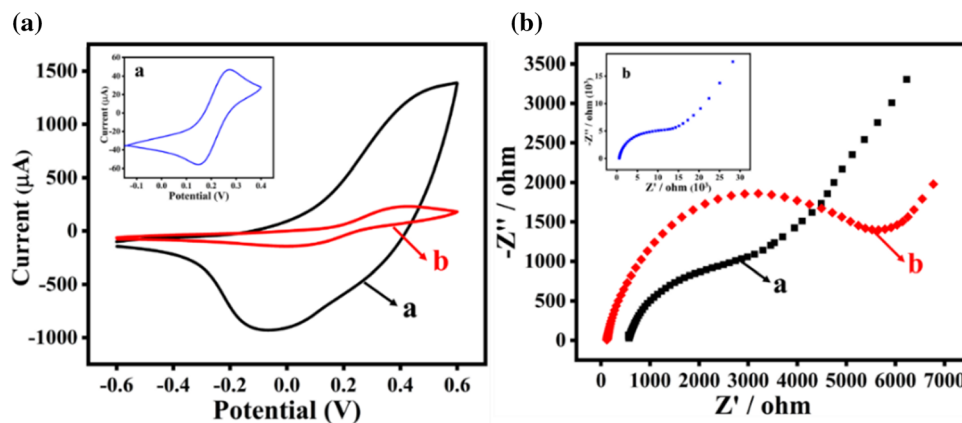
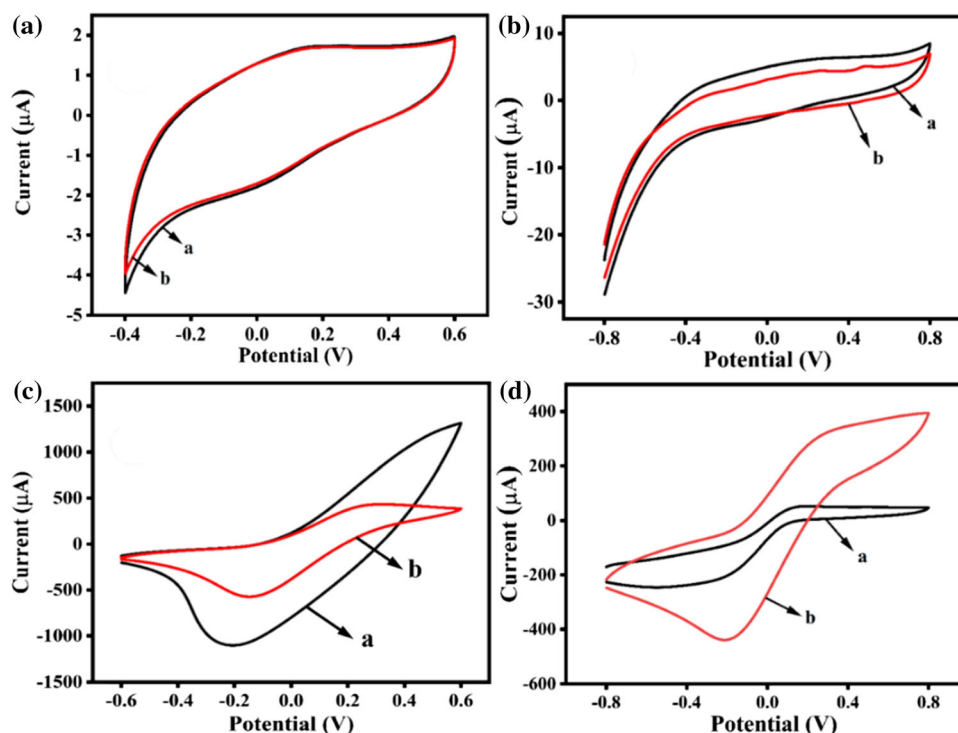


Figure 4 CVs of (A) bare GCE, (B) PANI/GCE, (C) PA-PANI/GCE and (D) PA-oPANI/GCE in 0.1 M Na_2HPO_4 -citrate buffer solution (pH 6.8) in the absence (a) and presence (b) of 40 ppb malathion at the scan rate of 100 mV s^{-1} .

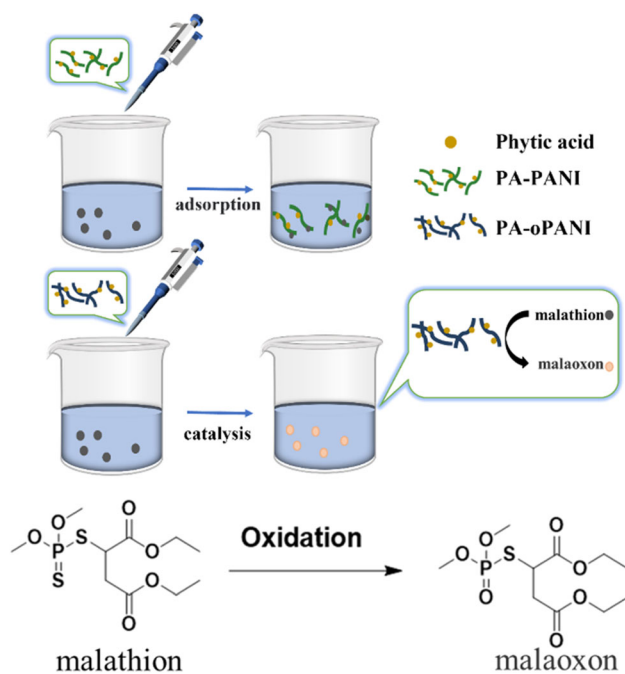
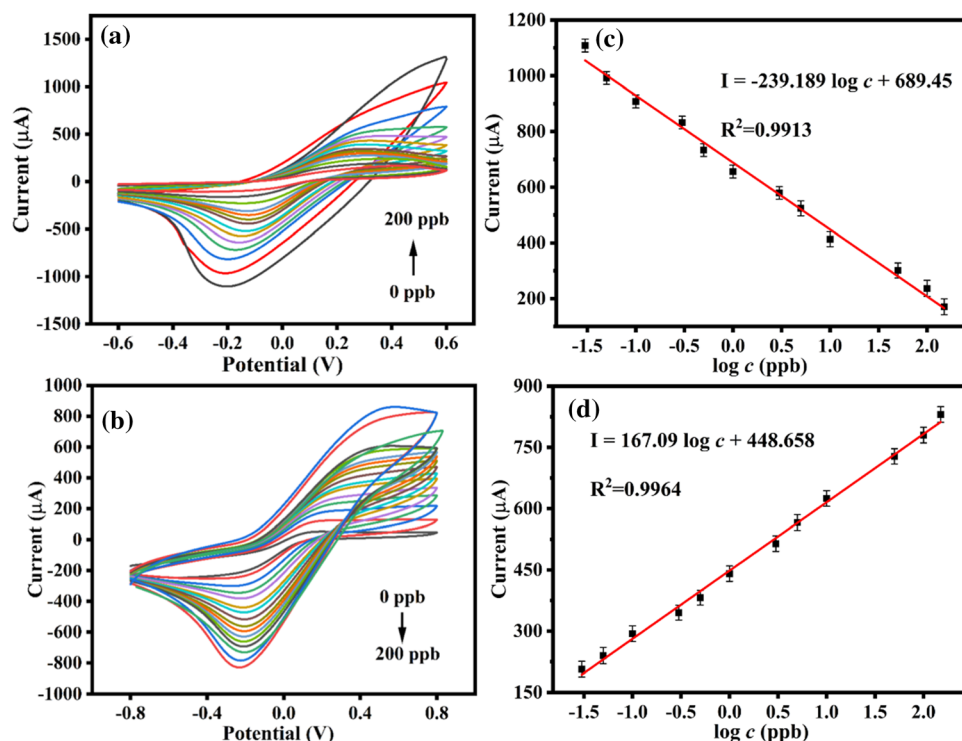


doping amount of PA from 0 to 0.46 mL, and decreased significantly at higher doping amount. Therefore, the PA doping amount of 0.46 mL was chosen as the optimal doping amount for the preparation of the electrochemical sensor. In addition, other important experimental parameters including pH of the Na_2HPO_4 -citrate buffer solution and concentration of dropped PA-PANI material were also evaluated in detail. The results demonstrated that pH value of 6.8 and PA-PANI concentration of 1.0 mg/mL were beneficial to improvement of outstanding detection performance for both sensors, which can be used in all subsequent experiments and next detection.

Under the optimized conditions, PA-PANI/GCE and PA-oPANI/GCE were used to detect malathion at different concentrations ranged from 0.01 to 200 ppb with CV. As shown in Fig. 5, the current response decreased for PA-PANI/GCE and increased for PA-oPANI/GCE with the malathion concentration, meaning different detection mechanisms from two sensors. It can be inferred that the PA-PANI material can adsorb malathion molecules. And malathion adsorbed on the electrode surface can in turn hinder the electron transfer ability between PA-PANI material and the GCE electrode, thus leading to a downward trend of the peak current. Unlike PA-

PANI material, PA-oPANI composite showed good electrocatalytic performance in the detection of malathion. Malathion generated electrons in the oxidation process, which in turn enhanced the reduction process of peroxide-state polyaniline and increased the reduction peak current. Therefore, with the increase in malathion concentration, the peak currents of PA-oPANI/GCE tend to increase. The proposed detection mechanism for both sensors are presented in Scheme 2. The resulting malaoxone is the intermediate product of malathion degradation and is more prone to hydrolysis and further degradation into non-toxic compounds [37–41]. Figure 5C, D presented the calibration curve of the peak current and malathion concentrations for PA-PANI/GCE and PA-oPANI/GCE, respectively. Both sensors exhibited good linear response to malathion in the concentration range of 0.01–200 ppb, with the regression equation of $I = -239.19 \log c + 689.45$ ($R^2 = 0.9913$) for PA-PANI/GCE and $I = 167.09 \log c + 448.65$ ($R^2 = 0.9964$) for PA-oPANI/GCE, respectively (I in μA , c in ppb). The detection limit was calculated to be 1.58 ppt for PA-PANI sensor and 2.23 ppt for PA-oPANI sensor ($S/N = 3$), which is much better than previous malathion sensors (shown in Table 1).

Figure 5 CVs of PA-PANI/GCE(A) and PA-oPANI/GCE (B) and calibration curves for the determination of malathion (C, D) in 0.1 M Na₂HPO₄-citrate buffer solution (pH 6.8) at different malathion concentrations at the scan rate of 100 mV s⁻¹.



Scheme 2 Detection mechanism of the malathion.

In order to further explore the detection mechanism of malathion, the typical currents response of malathion on PA-PANI/GCE and PA-oPANI/GCE electrodes were investigated by cyclic voltammetry at different scanning rates and the results are shown in

Fig. 6. With the scanning rate increased from 50 to 250 mV/s, the cathodic peak potentials of the modified electrode moved slightly to negative direction and the anodic peak potential moved to positive direction. And the redox peak currents of PA-PANI/GCE and PA-oPANI/GCE electrodes increased with the increasing of scanning rates. As displayed in Fig. 6C, the reduction peak current of PA-PANI/GCE is positively proportional to the scanning rate, and the linear equation is $i_c = -5.07v - 6.02$ ($R^2 = 0.995$), suggesting that the electrode reaction is a typical adsorption-controlled process. In Fig. 6D, the reduction peak current of PA-oPANI/GCE is proportional to the 1/2 power of scanning rate, and the linear equation is $i_c = -223.06 v^{1/2} - 5.99$ ($R^2 = 0.993$). According to this linear relationship, it can be concluded that the electrochemical reduction process on PA-oPANI/GCE is a typical diffusion-controlled process.

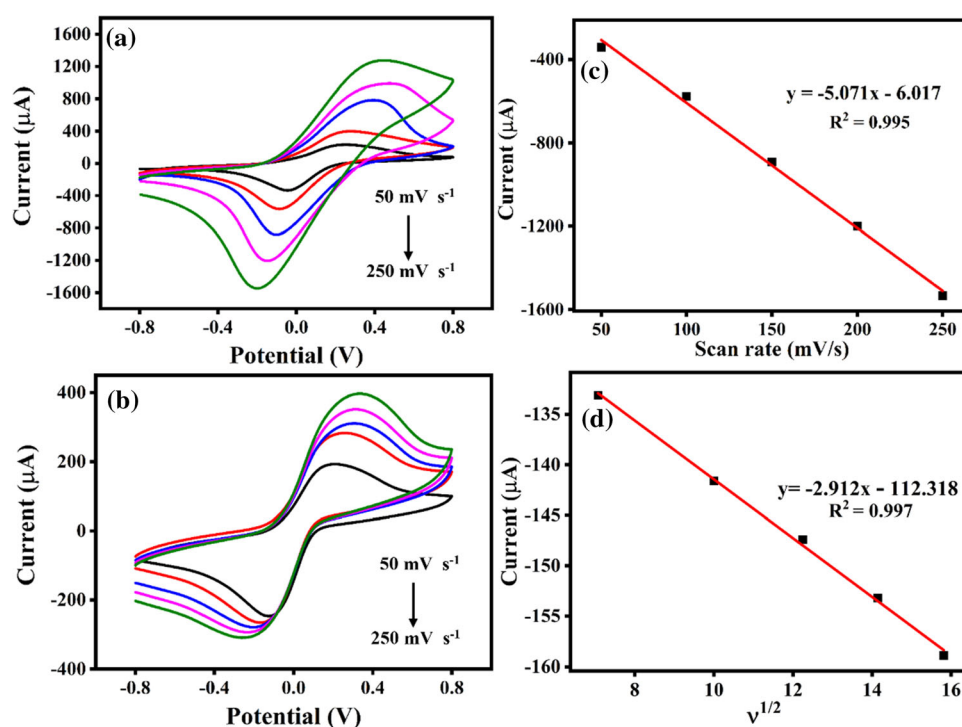
Stability, reproducibility and anti-interference ability

Stability, reproducibility and anti-interference ability are important parameters to evaluate the performance of electrochemical sensors. The reproducibility of the PA-PANI/GCE and PA-oPANI/GCE sensors

Table 1 Comparison of electrochemical response of different non-enzymatic malathion sensors

Modified materials	Detection method	Liner range	Detection Limit	References
CuO NPs/3DGR	DPV	0.03–1.5 nM	0.01 nM	[42]
FTO/PA6/polypyrrole	DPV	500– 2×10^4 ng/mL	0.8 ng/mL	[43]
c-MWCNT-CuO	CV	20–300 nM	0.143 nM	[44]
PANI-ES/SWCNTs/CPE	DPV	200–1400 nM	200 nM	[45]
Polyaniline/SWCNTs	DPV	0.2–1.4 nM	0.2 ng/mL	[38]
PA-PANI	CV	0.03–600 nM	0.0047 nM (1.58 ppt)	This work
PA-oPANI	CV	0.03–600 nM	0.0067 nM (2.23 ppt)	This work

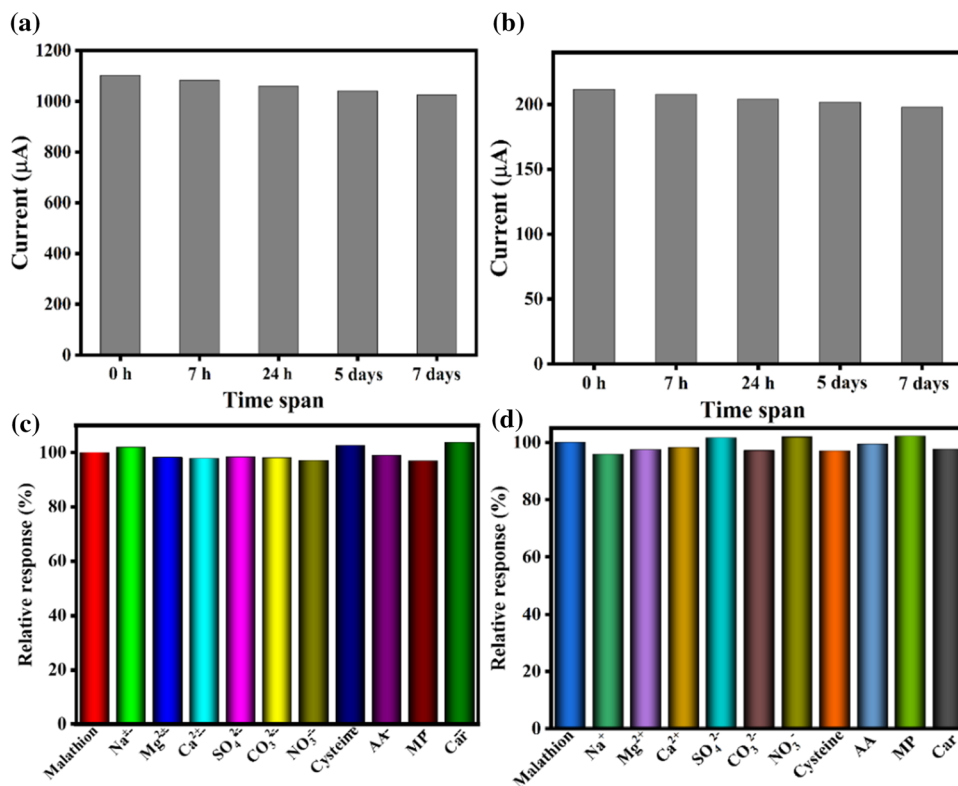
Figure 6 CVs of PA-PANI/GCE (A), PA-oPANI/GCE (B) at a scan rate of 50–250 mV s^{-1} in 0.1 M Na_2HPO_4 -citrate buffer solution (pH 6.8) containing 40 ppb malathion and corresponding linear relationship between scan rate and reduction peak current (C, D).



was investigated by 10 repeated assays of 10 ppb malathion under the same conditions, and the relative standard deviation (RSD) of response current were 1.3 and 2.9%, respectively. The results show that the electrochemical sensor has good reproducibility. To investigate long-term stability of PA-PANI/GCE and PA-oPANI/GCE electrochemical sensors, two electrodes were stored in ultrapure water at 4 °C for one week and its initial current response was measured at suitable intervals. As shown in Fig. 7A, B, the current response values changed little after one week, the PA-PANI/GCE sensor only decreased by 6.77%, and the PA-oPANI/GCE sensor only decreased by 6.51%, indicating that the two sensors have high environmental stability.

In order to study the anti-interference ability of the sensor, four kinds of common organic matter (5 times the concentration of malathion) and six kinds of common inorganic salt ions (10 times the concentration of malathion) were selected as interference substances, and then added to buffer solution for malathion detection. Generally, when the deviation of electrochemical signal is greater than 5%, it is judged that the foreign substance interferes with malathion detection. The obtained results are shown in Fig. 7. According to the result of Fig. 7C, the peak currents after addition of 50 ppb other organic compounds (ascorbic acid, methyl parathion, cysteine and carbendazim) in the presence of 10 ppb malathion were 102.6%, 96.89%, 98.9% and 103.63%, respectively, compared with the peak current

Figure 7 Study on stability of PA-PANI/GCE (A) and PA-oPANI/GCE (B) electrode. The current response of ultrapure water stored at 4 °C for 0 h, 7 h, 24 h, 5 days and 7 days, and selectivity studies of PA-PANI/GCE (C) and PA-oPANI/GCE (D) electrodes. Cyclic voltammograms experiments were performed with 0.1 M pH 6.8 Na_2HPO_4 -citrate buffer solution containing 10 ppb (30 nM) malathion in the absence and presence of 50 ppb ascorbic acid, methyl parathion, cysteine and carbendazim, 100 ppb Na^+ , Mg^{2+} , Ca^{2+} , SO_4^{2-} , CO_3^{2-} , NO_3^- , respectively.



obtained when malathion was only 10 ppb. These organic compounds did not interfere with the detection of malathion. In addition, when 100 ppb inorganic ions (Na^+ , Mg^{2+} , Ca^{2+} , SO_4^{2-} , CO_3^{2-} , NO_3^-) were added to buffer solution containing only 10 ppb malathion, the peak currents were 101.94%, 98.18%, 97.79%, 98.32%, 98.06% and 97.03% of 10 ppb malathion, which caused little interference to the sensor. The results showed that the PA-PANI/GCE sensor has good selectivity and anti-interference ability. Similarly, the PA-oPANI/GCE sensor shown in Fig. 7D also presented excellent selectivity and anti-interference ability.

Actual sample detection

To evaluate the applicability of the proposed electrochemical sensor, recoveries of MP concentrations were tested in the water samples by standard addition method. The water sample is obtained from East Lake of the Liaocheng University, Shandong, China. The supernatant obtained after precipitation was dispersed into Na_2HPO_4 -citrate buffer solution. Then three known concentrations of MP (5, 20 and 100 ppb for PA-PANI/GCE and 10, 40 and 160 ppb for PA-oPANI/GCE) were added to above solution for

electrochemical measurements and the detailed experimental results are presented in Table 2. The recovery values of MP were obtained from 95.16 to 117.3% for PA-oPANI/GCE and from 98.75 to 128% for PA-PANI/GCE, which indicated that the developed PA-oPANI/GCE and PA-PANI/GCE non-enzymatic malathion sensors have good reliability for MP detection in real water samples.

Conclusions

In conclusion, the novel electrochemical sensors based on PA and PANI composite material have been successfully developed for malathion determination.

Table 2 Recovery studies of MP in the water samples ($n = 3$)

Materials	Added (ppb)	Measured (ppb)	Recovery (%)
PA-PANI	5	6.4	128
	20	19.75	98.75
	100	102.7	102.7
PA-oPANI	10	11.73	117.3
	40	45.52	113.8
	160	152.27	95.16

Both of the PANI conductive states, intermediate state (PA-PANI) and peroxide state (PA-oPANI) can be used to construct electrochemical sensors with different detection mechanisms. The PA-PANI composite has a strong affinity for malathion, and malathion molecules absorbed can hinder electron transfer process of redox reactions of PANI molecules. The PA-oPANI composite presented excellent catalytic activity for the oxidation of malathion, thus enhancing the reduction process of peroxide-state PANI. The detection ability of the two electrodes was evaluated by CV tests, and both sensors showed excellent selectivity, wide linear range and low detection limits. The sensors are simple to prepare, economically feasible, good environmental stability, low detection limit, and has good specificity for the detection of malathion. It is expected to be a promising composite sensing platform for pesticide residue detection. Furthermore, the PA-oPANI/GCE sensor is regenerated by a peroxidation reaction after the detection of malathion. Further research on regenerative sensor applications is ongoing.

Acknowledgements

The authors are grateful for the support from the National Natural Science Foundation of China (21375055 and 21427808).

Author contributions

CH: conceptualization, investigation, data curation, formal analysis, writing—original draft. RY: conceptualization, supervision, writing—review and editing. QX: investigation, validation, writing—review and editing. SL: investigation, formal analysis. HW: writing—review and editing, supervision, project administration, funding acquisition.

Data availability

Data will be made available on request.

Declarations

Competing interests The authors declare that they have no known competing financial interests or

personal relationships that could have appeared to influence the work reported in this paper.

Ethics approval The study reported in this manuscript not involve ethical issues associated with human participants, their data or biological material and so on.

Supplementary Information: The online version contains supplementary material available at <http://doi.org/10.1007/s10853-022-08052-4>.

References

- [1] Wang J, Teng Y, Zhai Y, Yue W, Pan Z (2022) Spatiotemporal distribution and risk assessment of organophosphorus pesticides in surface water and groundwater on the north China plain, China. *Environ Res* 204:112310. <https://doi.org/10.1016/j.envres.2021.112310>
- [2] Eto M (2018) Organophosphorus pesticides: organic and biological chemistry. CRC Press
- [3] Berhanu S, Habtamu F, Tadesse Y, Gonfa F, Tadesse T (2022) Fluorescence sensor based on polyaniline supported Ag-ZnO nanocomposite for malathion detection. *J Sens* 2022:1–11. <https://doi.org/10.1155/2022/9881935>
- [4] Zhao X, Kong W, Wei J, Yang M (2014) Gas chromatography with flame photometric detection of 31 organophosphorus pesticide residues in *Alpinia oxyphylla* dried fruits. *Food Chem* 162:270–276. <https://doi.org/10.1016/j.foodchem.2014.04.060>
- [5] Valente NI, Tarelho S, Castro AL, Silvestre A, Teixeira HM (2015) Analysis of organophosphorus pesticides in whole blood by GC-MS- μ ECD with forensic purposes. *J Forensic Leg Med* 33:28–34. <https://doi.org/10.1016/j.jflm.2015.03.006>
- [6] da Silva GA, Augusto F, Poppi RJ (2007) Simultaneous optimization by neuro-genetic approach of a multiresidue method for determination of pesticides in *Passiflora alata* infuses using headspace solid phase microextraction and gas chromatography. *J Chromatogr A* 1138:251–261. <https://doi.org/10.1016/j.chroma.2006.10.075>
- [7] Pérez-Ruiz T, Martínez-Lozano C, Tomás V, Martín J (2005) High-performance liquid chromatographic assay of phosphate and organophosphorus pesticides using a post-column photochemical reaction and fluorimetric detection. *Anal Chim Acta* 540:383–391. <https://doi.org/10.1016/j.aca.2005.03.055>
- [8] Dorea HS, Tadeo JL, Sanchez-Brunete C (1996) Determination of organophosphorus pesticide residues in fruits by

- gas chromatography with ITD and NPD detection. *Chromatographia* 43:380–386. <https://doi.org/10.1007/BF02271015>
- [9] Erdođdu G (2003) A sensitive voltammetric method for the determination of diazinon insecticide. *J Anal Chem* 58:569–572. <https://doi.org/10.1023/A:1024120320359>
- [10] Zhang YC, Su L, Manuzzi D, de los MonterosJiaHuoLei HVEWZDQY (2012) Ultrasensitive and selective non-enzymatic glucose detection using copper nanowires. *Biosens Bioelectron* 31:426–432. <https://doi.org/10.1016/j.bios.2011.11.006>
- [11] Dong J, Hou JY, Jiang JX, Ai SY (2015) Innovative approach for the electrochemical detection of non-electroactive organophosphorus pesticides using oxime as electroactive probe. *Anal Chim Acta* 885:92–97. <https://doi.org/10.1016/j.aca.2015.05.033>
- [12] Rhouati A, Majdinasab M, Hayat A (2018) A perspective on non-enzymatic electrochemical nanosensors for direct detection of pesticides. *Curr Opin Electrochem* 11:12–18. <https://doi.org/10.1016/j.coelec.2018.06.013>
- [13] Krstić DZ, Čolović M, Bavcon kraljFrankoKrinulovićTrebšeVasić MMKPV (2008) Inhibition of AChE by malathion and some structurally similar compounds. *J Enzyme Inhib Med Chem* 23(4):562–573. <https://doi.org/10.1080/14756360701632031>
- [14] Bao J, Huang T, Wang ZN, Yang H, Geng XT, Xu GL, Hou CJ (2019) 3D graphene/copper oxide nano-flowers based acetylcholinesterase biosensor for sensitive detection of organophosphate pesticides. *Sens Actuators B Chem* 279:95–101. <https://doi.org/10.1016/j.snb.2018.09.118>
- [15] Wang K, Liu Q, Dai LN, Yan JJ, Ju C, Qiu BJ, Wu XY (2011) A highly sensitive and rapid organophosphate biosensor based on enhancement of CdS-decorated graphene nanocomposite. *Anal Chim Acta* 695:84–88. <https://doi.org/10.1016/j.aca.2011.03.042>
- [16] Gao XY, Gao Y, Bian CC, Ma HY, Liu HL (2019) Electroactive nanoporous gold driven electrochemical sensor for the simultaneous detection of carbendazim and methyl parathion. *Electrochim Acta* 310:78–85. <https://doi.org/10.1016/j.electacta.2019.04.120>
- [17] Zhang P, Sun TT, Rong SZ, Zeng D, Yu HW, Zhang Z, Pan HZ (2019) A sensitive amperometric AChE-biosensor for organophosphate pesticides detection based on conjugated polymer and Ag-rGO-NH₂ nanocomposite. *Bioelectrochemistry* 127:163–170. <https://doi.org/10.1016/j.bioelechem.2019.02.003>
- [18] Li YP, Zhang Y, Han GY, Xiao YM, Li MY, Zhou W (2016) An acetylcholinesterase biosensor based on graphene/polyaniline composite film for detection of pesticides. *Chin J Chem* 34:82–88. <https://doi.org/10.1002/cjoc.201500747>
- [19] Yang YQ, Asiri AM, Du D, Lin YH (2014) Acetylcholinesterase biosensor based on a gold nanoparticle–polypyrrole–reduced graphene oxide nanocomposite modified electrode for the amperometric detection of organophosphorus pesticides. *Analyst* 139:3055–3060. <https://doi.org/10.1039/C4AN00068D>
- [20] Beygisangchin M, Abdul Rashid S, Shafie S, Sadrolhosseini AR, Lim HN (2021) Preparations, properties, and applications of polyaniline and polyaniline thin films—a review. *Polymers*. <https://doi.org/10.3390/polym13122003>
- [21] Furukawa Y, Ueda F, Hyodo Y, Harada I, Nakajima T, Kawagoe T (1988) Vibrational spectra and structure of polyaniline. *Macromolecules* 21:1297–1305. <https://doi.org/10.1021/ma00183a020>
- [22] Gao XH, Jing XY, Li YF, Zhu J, Zhang ML (2018) Synthesis and characterization of phosphorized polyaniline doped with phytic acid and its anticorrosion properties for Mg–Li alloy. *J Macromol Sci A* 55:24–35. <https://doi.org/10.1080/10601325.2017.1387485>
- [23] Wu HH, Chang CW, Lu D, Maeda K, Hu C (2019) Synergistic effect of hydrochloric acid and phytic acid doping on polyaniline-coupled g-C₃N₄ nanosheets for photocatalytic Cr (VI) reduction and dye degradation. *ACS Appl Mater Interfaces* 11(39):35702–35712. <https://doi.org/10.1021/acami.9b10555>
- [24] Amir M, Ashkan Z (2012) Synthesis and characterization of conducting polyaniline nanocomposites containing ZnO nanorods. *Prog Nat Sci Mater Int* 22:73–280. <https://doi.org/10.1016/j.pnsc.2012.07.002>
- [25] Devi MR, Saranya A, Pandiarajan J, Dharmaraja J, Prithvikumaran N, Jeyakumaran N (2019) Fabrication, spectral characterization, XRD and SEM studies on some organic acids doped polyaniline thin films on glass substrate. *J King Saud Univ Sci* 31:1290–1296. <https://doi.org/10.1016/j.jksus.2018.02.008>
- [26] Duhan M, Kaur R (2019) Phytic acid doped polyaniline nanofibers: an advanced adsorbent for methylene blue dye. *Environ Nanotechnol Monit Manag* 12:100248. <https://doi.org/10.1016/j.enmm.2019.100248>
- [27] Ali MB, Wang F, Boukherroub R, Lei W, Xia M (2019) Phytic acid-doped polyaniline nanofibers-clay mineral for efficient adsorption of copper (II) ions. *J Colloid Interface Sci* 553:688–698. <https://doi.org/10.1016/j.jcis.2019.06.065>
- [28] Gao X, Yan R, Xu L, Ma HY (2018) Effect of amorphous phytic acid nanoparticles on the corrosion mitigation performance and stability of sol-gel coatings on cold-rolled steel substrates. *J Alloy Compd* 747:747–754. <https://doi.org/10.1016/j.jallcom.2018.03.078>
- [29] Golczak S, Kancierzewska A, Fahlman M, Langer K, Langer JJ (2008) Comparative XPS surface study of polyaniline

- thin films. *Solid State Ionics* 179:2234–2239. <https://doi.org/10.1016/j.ssi.2008.08.004>
- [30] Kumar SN, Gaillard F, Bouyssoux G, Sartre A (1990) High-resolution XPS studies of electrochemically synthesized conducting polyaniline films. *Synth Met* 36:111–127. [https://doi.org/10.1016/0379-6779\(90\)90240-L](https://doi.org/10.1016/0379-6779(90)90240-L)
- [31] Liu GL, Liu ZM, Li JL, Zeng M, Li ZY, He L, Li FW (2018) Chitosan/phytic acid hydrogel as a platform for facile synthesis of heteroatom-doped porous carbon frameworks for electrocatalytic oxygen reduction. *Carbon* 137:68–77. <https://doi.org/10.1016/j.carbon.2018.05.027>
- [32] Pan X, Wu S, Wang T, Histan G, Li Y (2022) Copper containing 3D polyaniline/phytic acid hydrogels for photocatalytic hydrogen production. *J Mater Sci* 57(27):12836–12847. <https://doi.org/10.1007/s10853-022-07424-0>
- [33] Zhang D, Yang J, Qiao G, Wang J, Li H (2021) Facile two-step synthesis of nanofiber polyaniline/graphene/cuprous oxide composite with enhanced photocatalytic performance. *Appl Nanosci* 11(3):983–993. <https://doi.org/10.1007/s13204-020-01660-z>
- [34] Bavastrello V, Terencio TBC, Nicolini C (2011) Synthesis and characterization of polyaniline derivatives and related carbon nanotubes nanocomposites—study of optical properties and band gap calculation. *Polymer* 52(1):46–54. <https://doi.org/10.1016/j.polymer.2010.10.022>
- [35] Sinha S, Bhadra S, Khastgir D (2009) Effect of dopant type on the properties of polyaniline. *J Appl Polym Sci* 112(5):3135–3140. <https://doi.org/10.1002/app.29708>
- [36] Almasi MJ, Sheikholeslami TF, Naghdi MR (2016) Band gap study of polyaniline and polyaniline/MWNT nanocomposites with in situ polymerization method. *Compos B Eng* 96:63–68. <https://doi.org/10.1016/j.compositesb.2016.04.032>
- [37] Khalid M, Acuna JJ, Tumelero MA, Fischer JA, Zoldan VC, Pasa AA (2012) Sulfonated porphyrin doped polyaniline nanotubes and nanofibers: synthesis and characterization. *J Mater Chem* 2:11340–11346. <https://doi.org/10.1039/C2JM31116J>
- [38] Ebrahim S, El-Raey R, Hefnawy A, Ibrahim H, Soliman M, Abdel-Fattah TM (2014) Electrochemical sensor based on polyaniline nanofibers/single wall carbon nanotubes composite for detection of malathion. *Synth Met* 190:13–19. <https://doi.org/10.1016/j.synthmet.2014.01.021>
- [39] Zhang YY, Xiao ZY, Chen F, Ge YQ, Wu JH, Hu XS (2010) Degradation behavior and products of malathion and chlorpyrifos spiked in apple juice by ultrasonic treatment. *Ultrason Sonochem* 17:72–77. <https://doi.org/10.1016/j.ultsonch.2009.06.003>
- [40] Yu H, Jian X, Jin J, Zheng XC, Liu RT, Qi GC (2015) Nonenzymatic sensing of glucose using a carbon ceramic electrode modified with a composite film made from copper oxide, overoxidized polypyrrole and multi-walled carbon nanotubes. *Microchim Acta* 182:157–165. <https://doi.org/10.1007/s00604-014-1310-x>
- [41] Yu H, Jin J, Jian X, Wang Y, Qi GC (2013) Preparation of cobalt oxide nanoclusters/overoxidized polypyrrole composite film modified electrode and its application in nonenzymatic glucose sensing. *Electroanalysis* 25:1665–1674. <https://doi.org/10.1002/elan.201300035>
- [42] Xie Y, Yu YH, Lu LM, Ma X, Yu YF (2018) CuO nanoparticles decorated 3D graphene nanocomposite as nonenzymatic electrochemical sensing platform for malathion detection. *J Electroanal Chem* 812:82–89. <https://doi.org/10.1016/j.jelechem.2018.01.043>
- [43] Migliorini FL, Sanfelice RC, Mercante LA, Facure MH, Correa DS (2019) Electrochemical sensor based on polyamide 6/polypyrrole electrospun nanofibers coated with reduced graphene oxide for malathion pesticide detection. *Mater Res Express* 7(1):015601
- [44] Seraga E, El-Maghraby A, Hassane N, El Nemra A (2021) CuO@MWCNTs nanocomposite as non-enzyme electrochemical sensor for the detection of malathion in seawater. *Desalin Water Treat* 236:240–249
- [45] Alabri AM, Abdul Halim SN, Abu Bakar NK, Saharin SM, Sherino B, Rashidi Nodeh H, Mohamad S (2019) Highly sensitive and selective determination of malathion in vegetable extracts by an electrochemical sensor based on Cu-metal organic framework. *Environ Sci Health B* 54:930–941. <https://doi.org/10.1080/03601234.2019.1652072>

Publisher's Note Springer Nature remains neutral with regard to jurisdictional claims in published maps and institutional affiliations.

Springer Nature or its licensor (e.g. a society or other partner) holds exclusive rights to this article under a publishing agreement with the author(s) or other rightsholder(s); author self-archiving of the accepted manuscript version of this article is solely governed by the terms of such publishing agreement and applicable law.